Chapter 7
Instrumentation for near-field scanning microwave microscopy

7.1 Introduction

In the preceding chapters, we have focused on broadband, calibrated measurements of nanoelectronic devices. In particular, we have described techniques for the measurement of calibrated, complex scattering parameters and the subsequent extraction of circuit model parameters. In order to facilitate the ongoing development of novel, radio-frequency (RF) nanoelectronic devices, it is highly desirable to complement scattering parameter measurements with local, intra-device measurements. Furthermore, non-destructive, spatially-localized characterization of nanomaterials and other nanoelectronic building blocks is critical for engineering of RF nanoelectronics. Thus, in this chapter, we introduce broadband, near-field probes, especially those integrated with scanning probe microscopes. Here, we consider the practical implementations of such scanning probe systems.

In designing a near-field scanning microwave microscope (NSMM) system, several critical questions must be considered. Will the probe be implemented with a resonant or non-resonant microwave circuit? What type of microwave probe will be used: a sharpened metal tip, a planar structure such as a stripline, or perhaps a resonant cavity with a sub-wavelength aperture? What distance-following mechanism will be used to maintain a constant separation between the probe and the sample under test? Depending on how these questions are addressed, any of a wide variety of NSMM designs may be engineered. In addition, the instrumentation directly impacts calibration techniques, which will be described in detail in the following chapter, as well as with the underlying physical models and theory of operation for NSMMs. Before proceeding to the detailed discussion of contemporary approaches to NSMM instrumentation, we will briefly review the historical development of near-field microwave probing.

7.2 Historical development

In an ideal, classical optical microscope, it has long been known that the resolution is limited by diffraction. The diffraction limit, also known as the Abbe limit, is on the order of λ, where λ is the wavelength of the probing illumination. More generally, it is extremely difficult to resolve sub-wavelength features with far-field systems in which the probe-sample distance r is much larger than both λ and the size of the illuminating source D. As a result, improvements in the resolution of far field microscopes have historically relied on the use of smaller and smaller wavelengths, pushing into the extreme-ultraviolet regime and below. Things are quite different in the near field. In particular, in the near-field regime, evanescent waves make a significant contribution to the total field and enable sub-wavelength resolution. Thus, a near field probe may be implemented by devising an

illuminating or field-focusing source of dimension D that illuminates at wavelength λ and is positioned a very short distance r from the probe, with $r << \lambda$.

An early proposal to implement a near field probe was made by Edward H. Synge in 1928 [1]. Synge proposed to create a probe by opening a sub-wavelength aperture in an otherwise opaque barrier that was positioned close to the sample of interest such that it was within the near field. An image could then be generated by scanning the aperture back and forth above the sample. Synge's probe concept won endorsement from Albert Einstein himself [2], but the instrumentation limits of his day prevented Synge from implementing his idea. Note that there is an important tradeoff required for implementation of such a near field probe. In the far-field, all points on an object within the field of view may be imaged simultaneously by use of far-field optics. In the near-field, an image can only be obtained by serially scanning the probe over the object and making a separate measurement at each probe position. Thus, the near-field strategy requires additional instrumentation for scanning and longer times for image acquisition. Experimental work in near-field microscopy did not emerge until the late 1960s and early 1970s. Bryant and Gunn demonstrated a probe-based microscope for measurement of the local resistivity of a semiconductor crystal with spatial resolution on the order of 1 mm [3]. Their system consisted of a sharpened probe integrated with a bridge-based impedance detector. In order to maximize the sensitivity of their system, the electrical length of the probe signal path was required to be equal to an integral number of half-wavelengths at the operation frequency (450 MHz), effectively creating a resonant circuit. Later, Ash and Nicholls produced an aperture-based microscope that was able to measure the local relative permittivity of dielectrics with 0.5 mm spatial resolution [4]. The central element of their apparatus was a 10 GHz resonator with a sub-wavelength aperture, 1.5 mm in diameter. With the aperture positioned directly above a dielectric sample, they measured shifts in both the quality factor Q and resonant frequency f_0 of the resonator as a function of local permittivity. Measurements of these two variables have since become a hallmark of NSMM measurement techniques.

Over the course of the intervening decades, numerous and varied implementations of NSMM systems and related tools have been reported [5],[6]. For example, several NSMM designs have been developed that combine microwave compatibility with the spatial resolution of vacuum scanning tunneling microscopy [7]-[9], pushing NSMM toward the atomic scale. Engineering and design of NSMM probes has also been an area of particular interest. Custom probe designs include fully microfabricated coaxial probes [10], field-focusing probes sculpted with a focused ion beam [11], and metal-coated nanowire probes [12], as shown in Fig. 7.1. These examples, along with the NSMM systems discussed below, represent but a small fraction of published implementations. While an exhaustive study of NSMM instrumentation is beyond the scope of this book, below we cite several representative systems that exemplify different design strategies and choices. Note that as a result of the ongoing development of NSMM instrumentation, several different NSMM systems are now commercially available.

Figure 7.1. **Specialized probes for near-field scanning microwave microscopy.** (a) Scanning electron microscope (SEM) image of the tip of a microfabricated coaxial probe. All components of the probe, including the cantilever body, the planar waveguide signal path, and the coaxial antenna probe, were constructed by following microfabrication techniques developed for microelectromechanical systems. Adapted with permission from Y. Q. Wang, A. D. Betterman, and D. W. van der Weide, *J. Vac. Sci. Technol. B* **25** (2007) pp. 813-816. Copyright 2007, American Vacuum Society. (b) SEM image of a balance stripline resonator probe. The stripline was formed by depositing Al layers on either side of a tapered quartz bar. The tapered end of the bar was then further shaped by use of a focused ion beam in order to further confine the fields near the probe tip. Adapted from V. V. Talanov, A. Scherz, R. L. Moreland, and A. R. Schwarz, *Appl. Phys. Lett.* **88** (2006) art. no. 134106, with permission from AIP Publishing. (c) SEM image of a GaN nanowire-based probe. The defect free, mechanically robust nanowire was inserted into the apex of a silicon microcantilever by use of a focused ion beam and a nanomanipulator. In order to form a continuous microwave signal path, a thin metal layer was subsequently deposited on the cantilever by use of atomic layer deposition. [12]

7.3 Probe and sample motion

7.3.1 Distance-following mechanisms

In general, NSMM measurements depend on the local impedance presented to the probe tip by the sample under test. This impedance depends not only on the sample's electromagnetic material properties, but also on the geometries and relative position of the probe and the sample. Thus, the distance between the probe tip and the sample, z, is a critical parameter for NSMMs. In some imaging modes, the probe tip is kept in direct contact with the sample (z = 0 nm), while in other modes z may be on the order of 1 nm. A distance- or height-following mechanism is integrated into most scanning probe systems in order to maintain a constant value of z while the tip is raster-scanned across the sample surface. In certain situations, it may be desirable to make height-dependent NSMM measurements over several orders of magnitude in z, spanning from 1 nm to as much as a few millimeters. At the outset of height-dependent measurements, the distance-following mechanism is used to establish an initial tip-sample distance. Subsequently, the height-dependent measurement may be carried out by increasing the tip-sample distance until the probe interaction with the sample is negligible.

Over the last several decades, as scanning probe microscopes have become workhorses for nanotechnology research and development, many distance-following strategies have been developed. Several distance following mechanisms are shown in Fig. 7.2. For example, in

the scanning tunneling microscope (STM) a metal tip is positioned within a nanometer or less of the sample [13]. When a potential difference is present between the tip and sample, a tunneling current flows between the tip and the sample due to quantum mechanical tunneling of electrons. In order to maintain this small distance, a feedback loop is used to adjust z in order to maintain a constant tunneling current between the tip and the sample, as illustrated in Fig. 7.2(a). STM-type feedback has been implemented in NSMMs [7], but such systems are limited to conducting and semiconducting samples. In order to extend STM to dielectric materials, radio frequency STMs have been developed. In place of the DC tunneling current, the feedback loops in radio frequency STMs maintain a constant amplitude of an odd harmonic signal that is generated by nonlinear behavior of the tunneling current [8], [14]. While STM provides lateral spatial resolution on the atomic-scale, extremely clean surfaces are required. This requires an ultra-high vacuum environment as well as *in situ* sample cleaning capabilities.

Distance-following strategies based on atomic force microscopes (AFMs) allow access to a wide variety of samples. In an AFM, the probe tip is integrated into a microcantilever beam. A simple approach to distance-following in this configuration is contact mode AFM, in which the probe is in direct contact with the sample, leading to a deflection of the microcantilever. Then, a feedback loop is used to adjust z in order to maintain a constant beam deflection, as shown in Fig. 7.2(b). One common approach for monitoring the deflection of the cantilever beam is the so-called beam-bounce approach, in which a laser is focused on a spot near the free end of the beam. The beam is reflected off the cantilever onto a quadrant photodetector. By monitoring the difference in intensities between different quadrants of the detector, both the beam deflection and torsion may be monitored. Interferometric optical detection or capacitive motion detection may also be used to monitor the deflection of the cantilever. As an alternative to contact mode AFM, dynamic, non-contact approaches have been developed. The earliest non-contact AFM modes drive resonant vibrations of the cantilever [15]. Changes in the vibration frequency and amplitude may be directly correlated to surface topography. Further innovations in non-contact AFM modified this approach to incorporate deliberate tapping of the surface with the probe tip [16]. To date, most AFM-based NSMM systems have utilized contact mode, but non-contact NSMM is highly desirable as it has the potential to reduce mechanical wear of both the probe tip and the sample.

Figure 7.2. **Examples of distance-following mechanisms.** (a) Schematic of a scanning tunneling microscope junction. An atomically sharp tip is placed a small distance z from a conducting sample. In constant current mode, a fixed potential difference V is applied between the tip and sample and a feedback loop adjusts z to maintain a constant tunneling current I. (b) Schematic of a contact-mode atomic force microscope. When the probe tip is in contact with the sample, the cantilever beam is deflected at an angle θ, which is measured by use of a laser that reflects off of the cantilever and onto a split or quadrant

photodetector. The feedback loop adjusts the cantilever height to maintain a constant deflection. (c) Schematic of shear-force detection, including a tuning fork in contact with a sharp NSMM probe. A feedback loop is used to adjust the probe-sample distance to maintain a constant vibration frequency or amplitude of the tuning fork. Reprinted from J. C. Weber, J. B. Schlager, N. A. Sanford, A. Imtiaz, T. M. Wallis, L. M. Mansfield, K. J. Coakley, K. A. Bertness, P. Kabos, and V. M. Bright, *Rev. Sci. Instrum.* **83** (2012) art. no. 083702, with permission from AIP Publishing.

Design choices for distance-following in an NSMM or related probe microscope are often dictated by the intended application. As an example, consider an experiment in which optical illumination is introduced in order to excite the sample, such as the optical illumination of a photoconductive system [17], [18]. In general, any external stimulus that leads to change of the local impedance can be detected by NSMM. Here, the excitation of additional carriers in the photoconductive material will be detected. Since photoconductive samples may be sensitive to stray optical illumination from beam bounce detection instrumentation, alternative, light-free approaches such as tuning-fork-based feedback may be necessary for distance following [17]. A schematic of a tuning-fork-based distance-following system is shown in Fig. 7.2(c). A quartz tuning fork is placed in mechanical contact with the probe tip. This may be done by use of a clamp or by directly integrating the probe tip with one of the tines of the tuning fork. The fundamental-mode resonance frequency of a typical quartz tuning fork is about 32 kHz and has a quality factor on the order of 1000. During operation, the fork vibrates at resonance, excited by ambient energy sources or in some cases, driven by an actuator. As the probe tip is brought within a few nanometers of sample, probe-sample interactions damp the vibrations. A feedback loop is used to adjust the probe-sample distance to maintain a constant vibration frequency or amplitude. A lock-in technique may be used to improve the sensitivity of the feedback system to small signals.

The distance-following strategy has significant ramifications for NSMM. The distance-following feedback loop provides a mechanism to visualize the sample geometry. By convention, the resulting images are almost always referred to as “topographic images,” regardless of which distance-following strategy has been implemented. However, as each of these strategies relies on a different physical interaction with the sample, subtle differences exist between different types of topographic images. Further complications are introduced due to the fact that apparent dimensions in topographic images may be functions of additional parameters, including scan speed, scan direction, and any electric potential difference between the probe and the sample. A detailed understanding of topographic imaging mechanisms is particularly important in the interpretation and analysis of NSMM images. As we point out elsewhere in this book, the capacitive contribution to an NSMM image is highly dependent on the tip-sample geometry as well as the electromagnetic material properties of the sample. Thus, any attempt to isolate the material properties from

the overall measurement requires knowledge of the sample geometry. A topographic image, often obtained simultaneously with the microwave signal image(s), is usually the primary source of knowledge about the apparent sample geometry. Furthermore, extraction of material properties required accurate modeling of the tip-sample system, including parasitic capacitance, as will be described in detail in Chapter 9.

The theory of Tershoff and Hamann, which builds upon previous work by Bardeen, provides one simplified approach to interpretation of STM topographic images. In the Bardeen formalism [19], the tunneling current I is given by

$$I = \frac{4\pi e}{\hbar}\sum_{\mu,\nu} f(E_\mu)[1 - f(E_\nu + eV)]\left|M_{\mu\nu}\right|^2 \delta(E_\mu - E_\nu) \quad , \tag{7.1}$$

where $f(E)$ is the Fermi function, $M_{\mu\nu}$ are the tunneling matrix elements between the states of the tip (Ψ_μ) and the sample (Ψ_ν), E_μ is the energy of the states Ψ_μ in the absence of tunneling, V is the potential difference between the tip and the sample, e is the electron charge, and h is Planck's constant. Assuming the electronic structure of the tip apex may be represented by an s-wave, Tersoff and Hamann have shown that Equation (7.1) implies [20]

$$\frac{dI}{dV} \propto \rho_S(\boldsymbol{r}, E_F + eV) \quad , \tag{7.2}$$

where ρ_S is the sample local density of states, $\boldsymbol{r}$ is the position of the probe tip apex, and E_F is the Fermi energy of the sample. In other words, contrast in STM topographic images arises from variations in the local electronic structure, namely the local density of states evaluated at the probe position. Though local electronic structure and geometric arrangement of matter in the sample are related, they are not identical. In fact, certain adsorbed species that reduce the local density of states appear as depressions in STM topographic images, though the species is in fact adsorbed on top of the surface.

In an AFM, a combination of distance-dependent forces governs the interaction between the probe tip and the sample. When the probe tip is extremely close to the sample, Pauli repulsion dominates. However, as the probe is retracted from the sample surface, attractive van der Waals-type forces quickly become the dominant interaction mechanism. This combination of attractive and repulsive forces can be described by a Lennard-Jones potential. A typical form is

$$V(z) = \phi\left[\left(\frac{z_0}{z}\right)^{12} - 2\left(\frac{z_0}{z}\right)^{6}\right] \quad , \tag{7.3}$$

where φ and z_0 are positive constants. An example of a Lennard-Jones potential is shown in Fig. 7.3. In contact-mode AFM, the probe-sample interaction is repulsive, while in non-contact mode the interaction is attractive. For other imaging modes, such as intermittent contact mode, the interaction may be more complex.

Figure 7.3. **Lennard-Jones potential.** The interaction between a cantilever probe, located a distance z above the sample, may be described by a Lennard-Jones potential. Shaded regions correspond to "contact AFM," in which the forces are purely repulsive, and "non contact AFM," in which attractive forces dominate.

Ultimately, the probe-sample interaction may be sensitive to a number of factors, including chemical interactions between the tip and the sample or the presence of a static electric or magnetic field in the junction. While simple models such as the Tersoff-Hamann STM theory may be modified to provide a more detailed picture of the probe-sample interaction, a more expedient approach is to characterize the probe-sample behavior empirically through measurements. In an STM-like system, the measurements would likely take the form of height-dependent current spectroscopy, while in an AFM-like system, the measurements would likely take the form of height dependent force spectroscopy, also known as a "force-distance curve." Another pragmatic approach to the problem is to engineer areas into the sample that are known to be free of topographic features. In Chapter 14, we will describe how the presence of flat regions in an NSMM image may be leveraged to empirically de-convolve material properties from topographic cross-talk.

7.3.2 Probe and sample positioning

While one may often refer to "retracting the tip" or "scanning the tip," in the case of NSMM systems, as well as other scanned probes that incorporate microwave circuits, in practice it is usually best to keep the probe fixed and move the sample with respect to the tip. This is due to the fact that the probe is usually connected directly to the microwave signal path. This path often incorporates cabling or other elements that are sensitive to bending or other mechanical disturbances. Repeated, large-scale motion of the microwave hardware can thus introduce instability in the measured magnitude and phase. As a result, many NSMMs contain two sets of positioning elements. The first is for small-scale, fine positioning up to a few micrometers. This small-scale set of positioners is usually implemented by use of piezoelectric transducers and may move the tip or the sample, depending on the implementation. Closed-loop scanning stages implement a feedback loop to maintain constant lateral fine positions, often by use of a capacitive sensor. The fine motion generates the scanning of the probe relative to the tip. The second set of positioning is for large-scale, coarse motion over length scales from a few micrometers to a few millimeters. This large-scale positioner is often implemented by use of a stepper motor and usually moves only the sample in order to improve stability and reduce uncertainty and drift in microwave measurements.

7.4 Microwave probes and circuits

7.4.1. Aperture probes versus tip probes

Recall that Synge's original near-field microscope concept relied upon an aperture in an opaque screen, placed at a small distance above the sample under test. When microwave radiation is incident upon such an aperture of sub-wavelength dimensions, the aperture spatially confines the microwave field, effectively focusing the field to sub-wavelength dimensions and enabling sub-wavelength resolution in the near field. Nearly two decades after Synge's proposal, Bethe developed a more complete, general analysis of diffraction of electromagnetic radiation by sub-wavelength holes [21]. As practical implementations of the near-field microscope concept were developed, an alternative approach to spatial confinement was realized. It was recognized that a microwave signal path terminating in a sharp, conducting point could serve as an aperture-free alternative. Imagine such a probe, having a conical shape, but terminated at its terminal apex by a hemisphere. If this hemisphere, the probe tip, has sub-wavelength electrical dimensions, then it may also serve as a field-focusing element in the near field regime. Both aperture-based and tip-based NSMM instruments have been realized, though tip-based designs are currently predominant.

The apparatus developed by Ash and Nicholls in 1972 is an example of a microscope that incorporates an aperture [4]. A schematic of their instrument is shown in Fig. 7.4. At resonance, the open resonator operates at a frequency f_0 and has a beam radius of w_0. An opaque diaphragm blocks the transmission of the beam onto the sample, save for a small aperture of radius r_0. The sample object is scanned in a raster pattern under the aperture and the reflected signal is mapped as a function of position to produce an image. In order to improve sensitivity, the sample was vibrated at a modulation frequency f_m and a lock-in technique was implemented with a phase sensitive detector. Furthermore, a low-noise amplifier and an amplifier tuned to f_m are incorporated into the receiving system. In the original work [4], the resonator operated at a frequency f_0 of 10 GHz, corresponding to a resonant wavelength λ_0 of 3 cm, and the aperture diameter r_0 was 0.75 mm. Given the relatively large spatial distances involved, neither precise distance following nor control of the aperture-sample distance along z were required. This simple, groundbreaking system was shown to resolve individual lines in a metallic grating with a line width of $\lambda_0/60$. The system was also able to resolve contrast between a region with a relative permittivity of 2.58 and a neighboring region with a relative permittivity of 2.24.

Figure 7.4. **A near-field scanning microwave microscope with an aperture probe.** A schematic diagram of the aperture-based microscope developed by Ash and Nicholls in 1972. The design builds upon the original ideas of E. H. Synge, first published in 1928. Reprinted by permission from Macmillan Publishers Ltd: Nature. E. A. Ash and G. Nicholls, *Nature* **237** (1972) pp. 510-512. Copyright 1972.

Tip-based NSMM designs provide an alternative to aperture-based designs. As many contemporary AFMs and STMs utilize sharpened points as probes, tip-based NSMMs can be readily adapted from existing scanning probe instruments. One approach to a tip-based NSMM design is to modify STM instrumentation to incorporate a microwave signal path [7], [8], [22]. STM relies on quantum mechanical tunneling of electrons from a needle-like probe to a bulk sample, thus making it a natural platform for developing an NSMM. Note that STM-based NSMM is not appropriate for all applications, as it requires a conducting sample and usually requires a vacuum environment.

A schematic of an STM-based NSMM is shown in Fig. 7.5 [7]. From an electrical point of view, there are three major components to this NSMM design. First, the probe tip is integrated into a $\lambda/2$ coaxial, transmission-line resonator. As we will discuss below, the use of a resonant circuit increases the sensitivity of an NSMM, though at the cost of being limited to a finite number of operating frequencies, namely the resonant frequency and higher harmonics. If a hollow capillary tube is used in place of the solid center conductor within the resonator, the tube may serve as a socket into which sharpened metal probe tips are inserted [23]. This provides a simple mechanism for probe replacement, should a tip become inadvertently bent or dulled by use. The resonant cavity is effectively terminated by the capacitively-coupled, RF port of a bias tee. The bias tee serves as an interface between the resonator and the other two major electrical components: the microwave electronics and the DC tunneling current circuit.

Figure 7.5. **A near-field scanning microwave microscope design based on a scanning tunneling microscope.** The Bias Tee serves as a junction between the three main electrical components of the microscope: the resonant probe, the DC STM electronics, and the microwave electronics. Reprinted from *Ultramicroscopy* **94**, A. Imtiaz and S. M. Anlage, "A novel STM-assisted microwave microscope with capacitance and loss imaging capability," pp. 209-216, Copyright 2003 with permission from Elsevier.

The microwave electronics include a source, which supplies a signal to the resonator at the resonant frequency f_0. The signal reflected from the resonator is transmitted to a diode detector by use of a directional coupler. The output of the diode detector serves as the input to a frequency-following feedback circuit that locks the source frequency to f_0. In order to lock onto the resonant frequency, a low-frequency (~3 kHz) signal f_{mod} is used to frequency modulate the signal from the microwave source. The low-frequency signal also serves as a reference for a lock-in amplifier. The output of the lock-in amplifier is then time-integrated and fed back to the frequency control of the microwave source. The time-integrated signal also serves as a measurement of the resonator frequency shift [24]. A second lock-in amplifier, referenced to twice f_{mod}, is used to extract the quality factor Q, though a calibration procedure is required to quantitatively convert the output of the second lock-in

to Q [25]. Thus, the feedback circuit is designed to output the shift in the resonant frequency and the resonator quality factor. Both of these measurands are sensitive to changes in the tip-sample impedance and, in turn, the local electromagnetic properties of the sample. As in conventional STM, the DC tunneling current circuit incorporates a feedback loop that serves as the distance-following mechanism. Specifically, in constant current mode, the DC tip-sample bias voltage is fixed and the feedback loop adjusts the tip-sample distance such that a constant tunneling current is maintained. For bias voltages in the range between millivolts and volts, corresponding tunneling currents typically are in the range between picoamps and nanoamps. The varying tip-sample distance is the topography signal. Thus, three types of images can be simultaneously obtained by this type of NSMM: a topographic image, a frequency shift image, and a quality factor image.

7.4.2 Resonant probes versus non-resonant probes

The preceding NSMM implementations, shown in Fig. 7.4 and Fig. 7.5, are examples of resonant probes. Resonant probes are formed by integrating the field-focusing feature (aperture or tip) into a resonant structure, such as a cylindrical cavity or a resonant microwave circuit. The motivation for this approach is clear: by integrating the probe into a resonant structure, the signal-to-noise ratio of the NSMM is improved by a factor of Q. On the other hand, a critical limitation of resonant NSMMs is that they necessarily operate at or near f_0 or, in some cases, harmonic multiples of f_0. Some leeway in the operating frequency can be obtained by introducing a tunable resonant structure, but this may require compromising the resonator's Q and, in turn, the signal-to-noise ratio of the NSMM. Applications of resonant NSMMs include measurements of permittivity and loss tangent in bulk solids [26] and liquids [27], as well as measurements of surface resistance in metallic thin films [28].

When the probe tip is positioned near a sample under test, the sample presents a load to the microwave resonator circuit, leading to perturbations of both the resonant frequency f_0 and quality factor Q. The magnitude of these perturbations will depend on the local, electromagnetic material properties of the sample, the sample geometry, and the vertical distance between the probe and the sample z. The dependence upon z suggests the most straightforward approach to resonant NSMM measurements: a height-dependent measurement of f_0 and Q. Initial, unperturbed values of f_0 and Q may be established by making a measurement while the resonant NSMM's probe tip is far from the sample. Although height-dependent NSMM measurements are at times referred to as "approach curves," in practice it is often useful to begin the measurement with the probe at its closest approach distance and then make measurements of f_0 and Q as the tip is retracted from the sample surface. Note that this requires measurement of the full spectral response at each height, in order to get a reliable fit and determination of f_0 and Q. This can be time consuming, and requires a high degree of mechanical stability as well as an accurate determination of the height z. Detailed methods to extract material properties from height-dependent NSMM measurements will be discussed in Chapter 9.

Another resonant NSMM implementation is shown in Fig. 7.6 [26]. The system is based on a quarter-wavelength coaxial resonator (f_0 ~ 1 GHz and Q ~ 1000) that is operated in transmission mode. A probe tip is mounted on the center conductor and protrudes through a small opening in the resonator. For this system, the probe consists of a metal wire, 50 μm to 100 μm in diameter, with the probe tip sharpened to sub-micrometer dimensions. In this implementation, a sapphire ring coated with a thin metal layer encircles the tip wire at the aperture in order to shield the resonator from far-field propagating components. The relative permittivity and loss tangent of single-crystal dielectrics have been extracted from measurements made with this type of NSMM. The extraction relies upon a quasistatic model of the probe-sample interaction that based on the method of images and yields values of material parameters that are in good agreement with values obtained by bulk characterization techniques [26], [29].

Figure 7.6. **A near-field scanning microwave microscope design based on a coaxial resonator.** (a) A schematic of the coaxial resonator, which is operated in transmission mode. (b) A closer view of the probe tip, which is connected to the center conductor of the resonator and extends toward the sample through an opening in the bottom of the resonator. Adapted from C. Gao and X.-D. Xiang, *Rev. Sci. Instrum.* **69** (1998) pp. 3846-3851, with permission from AIP Publishing.

Yet another implementation of a resonant NSMM is based on a two-dimensional, stripline resonator in place of the resonant cavity [30]. To fabricate the probe, a half-wavelength stripline resonator (f_0 ~ 1 GHz) is patterned on a dielectric substrate, as shown in Fig. 7.7(a). One end of the resonator is capacitively coupled to the RF source. The other end of the resonator is tapered and terminates in a sharpened point that extends beyond the end of the dielectric substrate, forming the probe. A second dielectric layer is added above the patterned resonator and ground planes are added to the top and bottom to complete the structure, as shown in Fig. 7.7(b). In Reference [30], the NSMM is operated in reflection mode. The reflected RF signal is separated from the incident signal by use of a three-port circulator and measured by use of a crystal detector. Furthermore, the sensitivity of the instrument is increased by modulating the sample position at a low frequency (100 Hz) and the use of a lock-in technique. Relative to cavity, coaxial, and rectangular waveguide resonators, stripline resonators offer the advantage of low cost and compact footprint. However, as with many planar transmission structures, striplines may radiate into free space, potentially causing unwanted effects depending on the experimental conditions.

Figure 7.7. **A near-field scanning microwave microscope design based on a planar stripline resonator.** (a) A schematic revealing the center plane of the probe structure,

including the stripline resonator integrated with a probe tip. The feedline is capacitively coupled to the resonator. (b) Side view of the probe structure after a second set of dielectric and ground plane layers has been added on top of the center plane. Adapted from M. Tabib-Azar, D.-P. Su, A. Pohar, S. R. LeClair, and G. Ponchak, *Rev. Sci. Instrum.* **70** (1999) pp. 1725-1729, with permission from AIP Publishing.

Beyond the examples described above, there are numerous alternative implementations of resonant NSMM systems. In addition to providing improved signal-to-noise, the resonant elements of these NSMM systems are generally well-understood and their electrical performance and electromagnetic field structure can be precisely engineered. Furthermore, modeling of these systems is often simplified by the use of well-established, lumped-element models for resonant cavities and circuits. In recent years, a number of NSMM designs have been realized without the inclusion of an engineered resonant structure in the microwave circuit. These non-resonant NSMMs follow many of the same operational principles as resonant NSMMs and display many of the same advantages. From an instrumentation and design perspective, non-resonant NSMMs may be easier to implement in that they require only a microwave signal path to the probe tip with relatively low loss, without the need for a specific resonant structure or circuit. This advantage is particularly important if an existing scanning probe microscope platform is retro-fitted or modified to work in an NSMM mode.

When a one-port microwave network is incorporated into a scanning probe microscope, the reflection coefficient will be frequency-dependent. This frequency dependence will be determined not only by the load impedance, but also by the physical implementation of the signal path, including cable connections, adapters, and the transition from a guided wave structure to the probe tip. The cumulative effect of these interfaces and the associated impedance mismatches is that sharp mimima in the reflection coefficient exist at selected frequencies. An example of such a minimum is shown by the solid curve in Fig. 7.8. This minimum resembles a resonance and an effective "resonant" frequency f_0 and effective quality factor Q may be assigned to the curve by fitting the curve with an appropriate function, e.g. a Lorentzian function. However, it should be noted that these minima represent frequencies at which the microwave network is well-matched to the source impedance rather than a true resonance. As with a resonant NSMM, when the probe tip of a non-resonant NSMM is brought near a sample under test, the shape of the local minimum will be altered, leading to shifts in f_0 and Q. The sign and magnitude of these shifts will depend sensitively upon the local sample impedance.

Figure 7.8. **Operating conditions for a near-field scanning microwave microscope.** A local minimum in the magnitude of the reflection coefficient ($|S_{11}|$) at 2.41 GHz is illustrated. This original peak (black curve) may be shifted during operation to a new

position (grey curve) due to vertical movement of the probe or lateral movement to a different area of the sample. If the system is operated at the minimum (here, 2.41 GHz), then the measured changes are ambiguous: based on $|S_{11}|$ measurements at a single frequency, the user will be unable to distinguish shifts to lower frequency from shifts to higher frequency. To overcome this, an off-peak operating frequency is chosen, as illustrated by the dashed, vertical line.

In practice, there will be multiple minima in the reflection coefficient that will work as operating frequencies for the NSMM. For example, Imtiaz, et. al. imaged a semiconductor reference sample at 2.3 GHz, 5.0 GHz, 9.6 GHz, 12.6 GHz, and 17.9 GHz with a non-resonant, commercial NSMM and observed frequency-dependent contrast in the resulting images [31]. The NSMM sensitivity may vary strongly for different operating frequencies and some local minima may be unsuitable as NSMM operating points. In a non-resonant system, the most effective operating frequencies are often found by trial and error. To optimize the NSMM sensitivity to the reflection coefficient, a tunable phase shifter may be inserted into the microwave signal path, between the source and the probe. With the probe out of contact, the phase shifter can be tuned to sharpen the local minimum in the reflection coefficient.

A full description of the position-dependent shifts in frequency and quality factor requires a complete measurement of the reflection coefficient as a function of frequency at each point of interest (Techniques for extracting quantitative material parameters from such measurements are described in Chapter 9). Such an approach is comprehensive, but impractical for most applications due to time and stability constraints. A practical alternative is to select a single operating frequency that is near, but not equal to f_0, as illustrated in Fig. 7.8. The magnitude and phase of the reflection coefficient are then measured at each probe position to generate images. Recall that the local minima that are used to establish the operating frequency occur when the microwave network is well-matched to the source impedance. Thus, barring *a priori* knowledge about whether the local impedance will result in better or poorer impedance matching, the direction of the shift in f_0 will initially be unknown for a given NSMM and a given sample. However, by operating at frequency offset from f_0 (on one side of the "resonance" curve), the contrast is unambiguous. In order to quantitatively map shifts in f_0 and Q to material parameters, it is necessary to phenomenologically validate a tip-sample model by use of a known reference or calibration sample, which will be introduced in Chapter 8.

7.5 Other aspects of near-field scanning microwave microscope instrumentation

So far, we have focused on two aspects of NSMM design and implementation in some detail: mechanical positioning and microwave electronics. Though these two aspects are particularly important for NSMM, a successful instrument requires engineering several additional subsystems, including environmental control, noise reduction, and thermal

control. Fortunately, many of the required techniques and methods have been previously developed for other scanning probe microscopes and microwave measurement systems. Environmental and noise issues have been addressed to varying degrees in the instrumentation examples discussed above. Here, we will briefly review three additional, specialized scanning probe microscope examples. Readers who are developing their own, customized NSMM systems are encouraged to consult the vast literature on this topic for a more comprehensive review of scanning probe microscope designs.

In Reference [8], Kemiktarak, *et al* described an implementation of a radio-frequency scanning tunneling microscope (RFSTM) that operates at cryogenic temperatures at megahertz frequencies and enables sensitive measurement of high frequency mechanical motion. The system utilizes a resonant circuit design, incorporating the resistive tunnel junction with an LC tank circuit to produce a resonant frequency of about 115 MHz. Specifically, the probe tip is fixed on a printed circuit board, which also includes the tank circuit, a bias tee, and a directional coupler. In this way, these components are necessarily located close to the tunnel junction and within the cryostat, thus reducing both signal loss and thermal noise. The low-temperature environment is further leveraged by incorporating a cryogenic amplifier into the radio frequency output path. The sensitivity of the RFSTM to mechanical motion was demonstrated by measuring the eigenfrequencies of a micromechanical resonator between 1.0 MHz and 3.0 MHz. Furthermore, topographic imaging based on measurement of the RF reflection coefficient enabled a 100-fold improvement in scan speed relative to conventional constant current STM imaging.

High speed imaging with scanning probe microscopes is a tantalizing prospect. Because of its subsurface imaging capability and compatibility with liquid environments, AFM-based NSMM is a promising tool for measurements of biologically important systems. However, progress in this area has been slow. Recently, AFM imaging at a rate of five frames per second has been demonstrated, capturing the motion of a myosin V molecule walking on an actin filament [32]. In order to achieve relatively high frame rates, specialized scanning techniques were implemented, including active damping of the scanner to reduce mechanical noise and optimization of the feedback electronics to enable high speed operation. In addition, the size of the AFM cantilever was reduced in order to increase the mechanical resonance frequency. While such advances in high-speed scanning have yet to be adopted in an NSMM design, many potential applications of high speed NSMM exist, including real time observation of subsurface processes occurring beneath membranes.

Subsurface imaging of liquids and other soft matter with NSMM can be furthered by customized sample containment. Custom sample cells have long been used for containing and imaging liquids within the vacuum environment of electron microscopes. Recently, Tselev *et al* developed a silicon-based cell for imaging processes in liquids with NSMM [33]. The liquid is encapsulated within a silicon well that is covered by a dielectric membrane (50 nm-thick silicon nitride or 8 nm-thick silicon dioxide). The NSMM probe tip scans along the flat surface of the membrane. Since the membrane is a dielectric, it functions as a

microwave-transparent window. In this configuration, electrochemical processes were imaged with an estimated lateral resolution of 250 nm. In separate experiments, yeast cells immersed in glycerol were imaged and the NSMM probe-depth was estimated to be a few hundred nanometers.

The field of near-field scanning microwave microscopy has grown rapidly in recent years and now incorporates a wide variety of microscopy techniques and instruments. The field of scanning probe microscopy is broader still. Here, we have illustrated several core choices required for effective design of an NSMM system by use of a small number of examples. Naturally, as the field moves forward, additional designs and imaging modes will emerge.

References

[1] E. H. Synge, "A suggested method for extending microscopic resolution into the ultra-microscopic region," *Philosophical Magazine Series 7*, **6**, No. 35, (1928) p. 356.

[2] M. Berry, E. Wolf, N. Bloembergen, N. Erez, and D. Greenberger, *Progress in Optics volume 50* (Elsevier, 2007) pp. 145-148.

[3] C. Bryant and J. Gunn, "Noncontact technique for the local measurement of semiconductor resistivity," *Review of Scientific Instruments*, **36** (1965) pp. 1614-1617.

[4] E. A. Ash and G. Nicholls, "Super-resolution aperture scanning microscope," *Nature*, **237**, (1972) pp. 510-512.

[5] A. Imtiaz, T. M. Wallis, and P. Kabos, "Near-field Scanning Microwave Microscopy," *IEEE Microwave Magazine* **15** (2014) pp. 52-64.

[6] B. T. Rosner and D. W. van der Weide, "High-frequency near-field micrsocopy," *Review of Scientific Instruments* **73** (2002) pp. 2505-2525.

[7] A. Imtiaz and S. M. Anlage, "A novel STM-assisted microwave microscope with capacitance and loss imaging capability," *Ultramicroscopy* **94** (2003) pp. 209-216.

[8] U. Kemiktarak, T. Ndukum, K. C. Schwab, and K. L. Ekinci, "Radio-frequency scanning tunneling microscopy," *Nature* **450** (2007) pp. 85-88.

[9] J. Lee, C. J. Long, H. Yang, X.-D. Xiang, and I. Takeuchi, "Atomic resolution imaging at 2.5 GHz using near-field microwave microscopy," *Applied Physics Letters* **97** (2010) art. no. 183111.

[10] Y. Q. Wang, A. D. Betterman, and D. W. van der Weide, "Process for scanning near-field microwave microscope probes with integrated ultratall coaxial tips," *Journal of Vacuum Science and Technology B* **25** (2007) pp. 813-816.

[11] V. V. Talanov, A. Scherz, R. L. Moreland, and A. R. Schwarz, "A near-field scanned microwave probe for spatially localized electrical metrology," *Applied Physics Letters* **88** (2006) art. no. 134106.

[12] J. C. Weber, P. T. Blanchard, A. W. Sanders, J. C. Gertsch, S. M. George, S. Berweger, A. Imtiaz, K. J. Coakley, T. M. Wallis, K. A. Bertness, N. A. Sanford, P. Kabos, and V. M. Bright, "GaN nanowire coated with atomic layer deposition of tungsten: A probe for near-field scanning microwave microscopy" *Nanotechnology* **25**, (2014) art. no. 415502.

[13] G. Binnig and H. Rohrer, "Scanning tunneling microscopy," *Surface Science* **126** (1983) pp. 1-3.

[14] G. P. Kochanski, "Nonlinear alternating-current tunneling microscopy," *Physical Review Letters* **62** (1989) pp. 2285-2288.

[15] Y. Martin, C. C. Williams, H. K. Wickramasinghe, "Atomic force microscope force mapping and profiling on a sub 100-Å scale," *Journal of Applied Physics* **61** (1987) pp. 4723-4729.

[16] Q. Zhong, D. Inniss, K. Kjoller, V. B. Elings, "Fractured polymer/silica fiber surface studied by tapping mode atomic force microscopy" *Surface Science Letters* **290** (1993) pp. L688.

[17] J. C. Weber, J. B. Schlager, N. A. Sanford, A. Imtiaz, T. M. Wallis, L. M. Mansfield, K. J. Coakley, K. A. Bertness, P. Kabos, and V. M. Bright, "A near-field scanning microwave microscope for characterization of inhomogeneous photovoltaics," *Review of Scientific Instruments* **83** (2012) art. no. 083702.

[18] A. Hovsepyan, A. Babajanyan, T. Sargsyan, H. Melikyan, S. Kim, J. Kim, K. Lee, and B. Friedman, "Direct imaging of photoconductivity of solar cells using a near-field scanning microwave microprobe," *Journal of Applied Physics* **106** (2009) art. no. 114901.

[19] J. Tersoff and D. R. Hamann, "Theory of the scanning tunneling microscope," *Physical Review B* **31** (1985) pp. 805-813.

[20] J. Tersoff and D. R. Hamann, "Theory and application for the scanning tunneling microscope," *Physical Review Letters* **50** (1983) pp. 1998-2001.

[21] H. A. Bethe, "Theory of diffraction by small holes," *Physical Review* **66** (1944) pp. 163-182.

[22] M. Farina, D. Mencarelli, A. Di Donato, G. Venanzoni, and A. Morini, "Calibration Protocol for Broadband Near-Field Microwave Microscopy," *IEEE Transactions on Microwave Theory and Techniques* **59** (2011) pp. 2769-2776.

[23] A. Imtiaz, *Quantitative Materials Contrast at High Spatial Resolution with a Novel Near-Field Scanning Microwave Microscope*, Ph.D. Dissertation, U. of Maryland (2005).

[24] D. E. Steinhauer, C. P. Vlahacos, S. K. Dutta, F. C. Wellstood, and S. M. Anlage, "Surface resistance imaging with a scanning near-field microwave microscope," *Applied Physics Letters* **71** (1997) pp. 1746-1738.

[25] D. E. Steinhauer, C. P. Vlahacos, S. K. Dutta, B. J. Feenstra, F. C. Wellstood, and S. M. Anlage, "Quantitative imaging of sheet resistance with a scanning near-field microwave microscope," *Applied Physics Letters* **72** (1998) pp. 861-863.

[26] C. Gao and X.-D. Xiang, "Quantitative microwave near-field microscopy of dielectric properties," *Review of Scientific Instruments* **69**, (1998) pp. 3846-3851.

[27] A. P. Gregory, J. F. Blackburn, K. Lees, R. N. Clarke, T. E. Hodgetts, S. M. Hanham, and N. Klein, "A Near-Field Scanning Microwave Microscope for measurement of th permittivity and loss of high-loss materials," *2014 84th ARFTG Microwave Measurement Symposium*, (2014) pp. 1-8.

[28] J. Kim, K. Lee, B. Friedman, and D. Cha, "Near-field scanning microwave microscopy using a dielectric resonator," *Applied Physics Letters* **83** (2003) pp. 1032-1034.

[29] C. Gao, T. Wei, F. Duewer, Y. Lu, and X.-D. Xiang, *Applied Physics Letters* **71**, (1997) pp. 1872-1874.

[30] M. Tabib-Azar, D.-P. Su, A. Pohar, S. R. LeClair, and G. Ponchak, "0.4 μm spatial resolution with 1 GHz (l = 30 cm) evanescent microwave probe," *Review of Scientific Instruments* **70** (1999) pp. 1725-1729.

[31] A. Imtiaz, T. M. Wallis, S.-H. Lim, H. Tanbakuchi, H.-P. Huber, A. Hornung, P. Hinterdorfer, J. Smoliner, F. Kienberger, and P. Kabos, "Frequency-selective contrast on variably doped p-type silicon with a scanning microwave microscope," *Journal of Applied Physics* **111** (2012) art. no. 093727.

[32] N. Kodera, D. Yamamoto, R. Ishikawa, and T. Ando, "Video imaging of walking myosin V by high-speed atomic force microscopy," *Nature* **468** (2010) pp. 72-76.

[33] A. Tselev, J. Velmurugan, A.V. Ievlev, S.V. Kalinin and A. Kolmakov. "Seeing through Walls at the Nanoscale: Microwave Microscopy of Enclosed Objects and Processes in Liquids," *ACS Nano* **10** (2016) pp. 3562-3570.

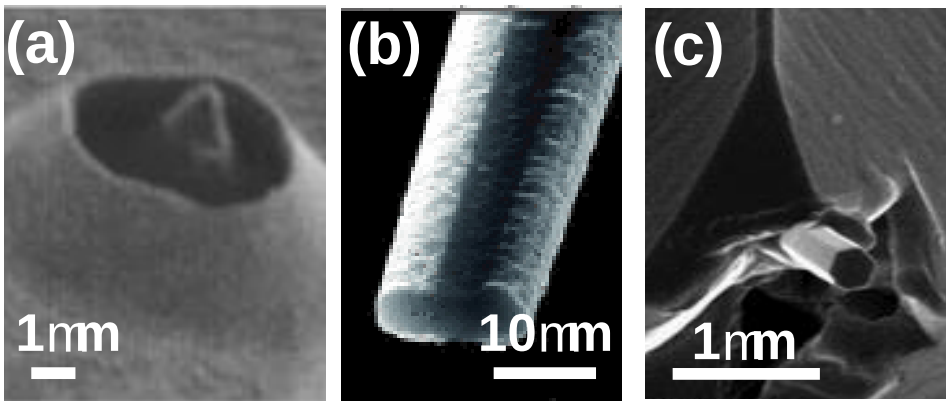

FIGURE 7.1

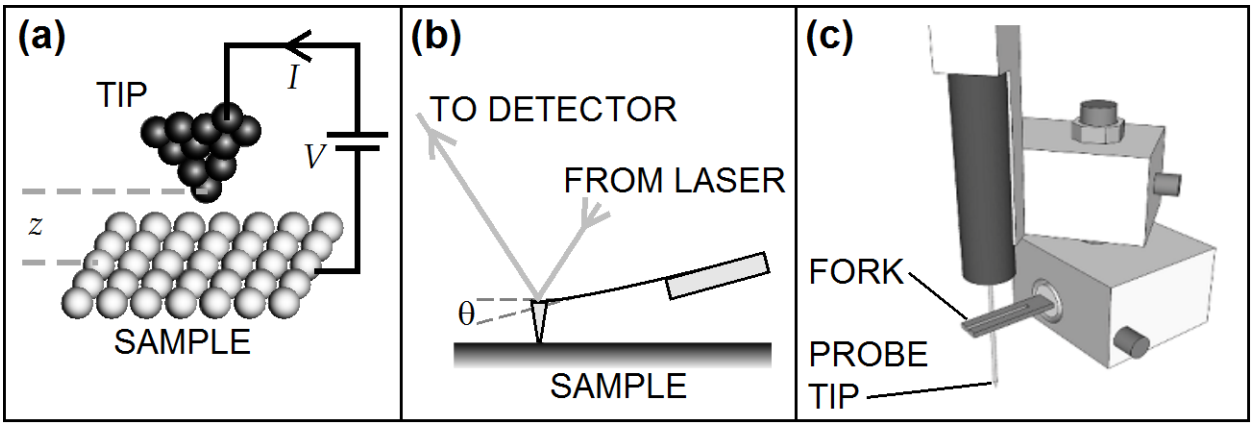
(a)
TIP
I
V
z
SAMPLE
(b)
TO DETECTOR
FROM LASER
θ
SAMPLE
(c)
FORK
PROBE
TIP

FIGURE 7.2

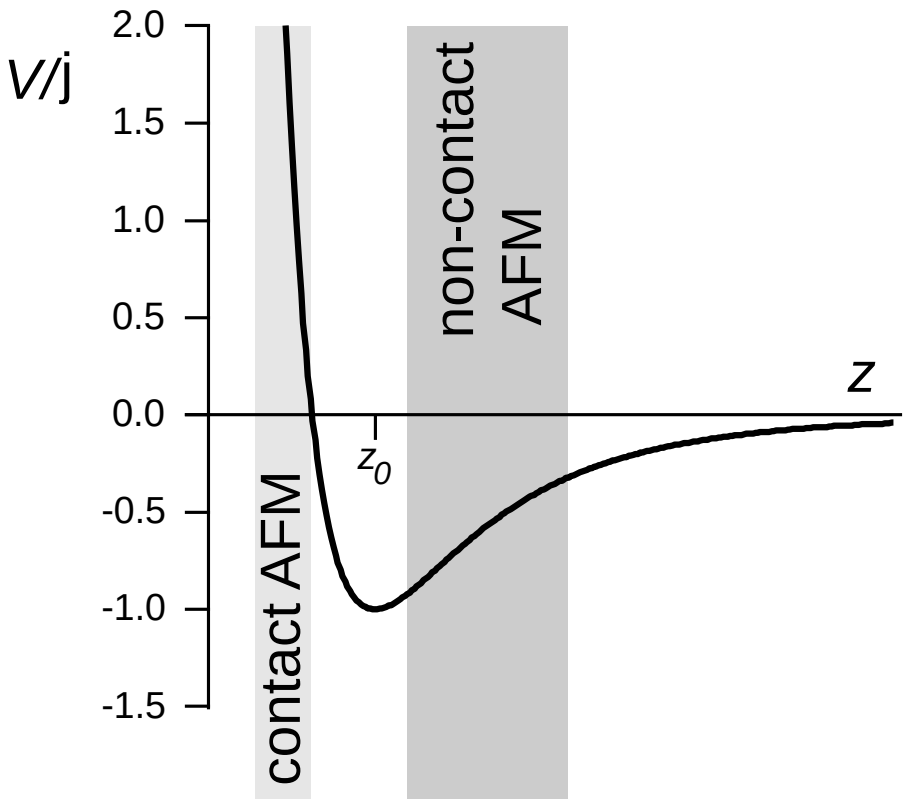

Figure 7.3

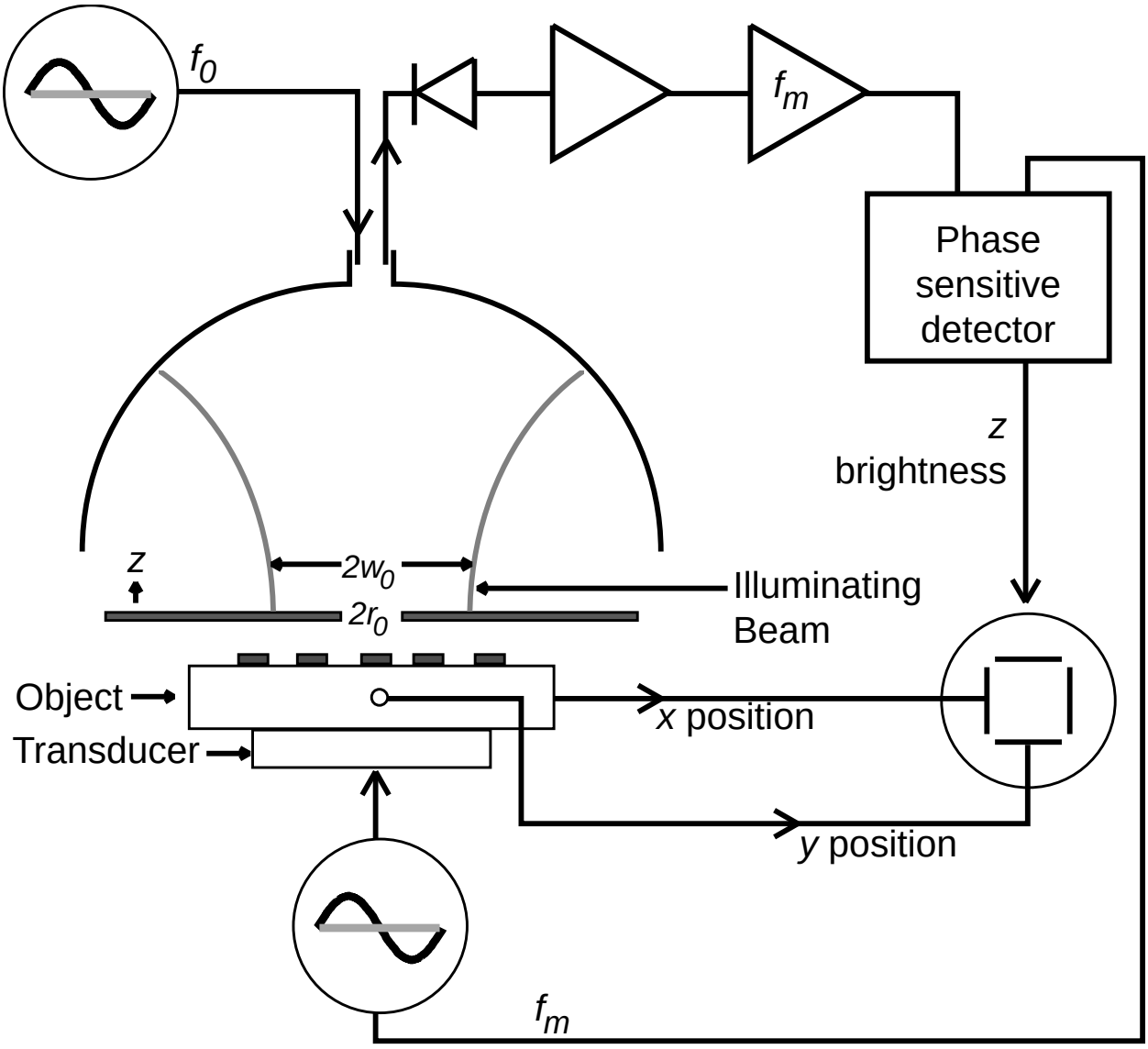
f_0
f_m
Phase sensitive detector
z
brightness
z
$2w_0$
$2r_0$
Illuminating Beam
Object
Transducer
x position
y position
f_m

Figure 7.4

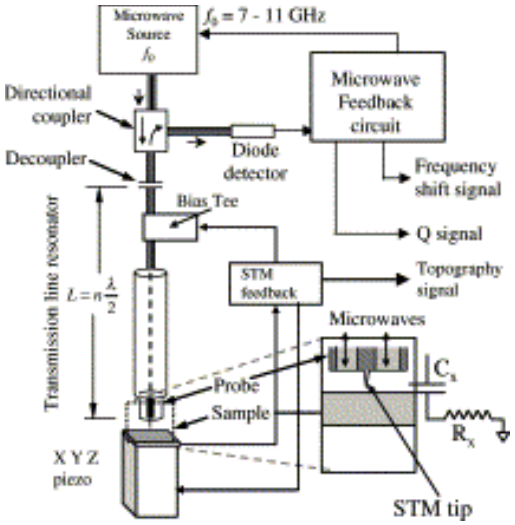
Microwave Source
$f_0 = 7 - 11$ GHz
Directional coupler
Decoupler
Diode detector
Microwave Feedback circuit
Frequency shift signal
Q signal
Bias Tee
STM feedback
Topography signal
Transmission line resonator
$L = n\frac{\lambda}{2}$
Microwaves
Probe
Sample
C_x
R_x
X Y Z piezo
STM tip

Figure 75

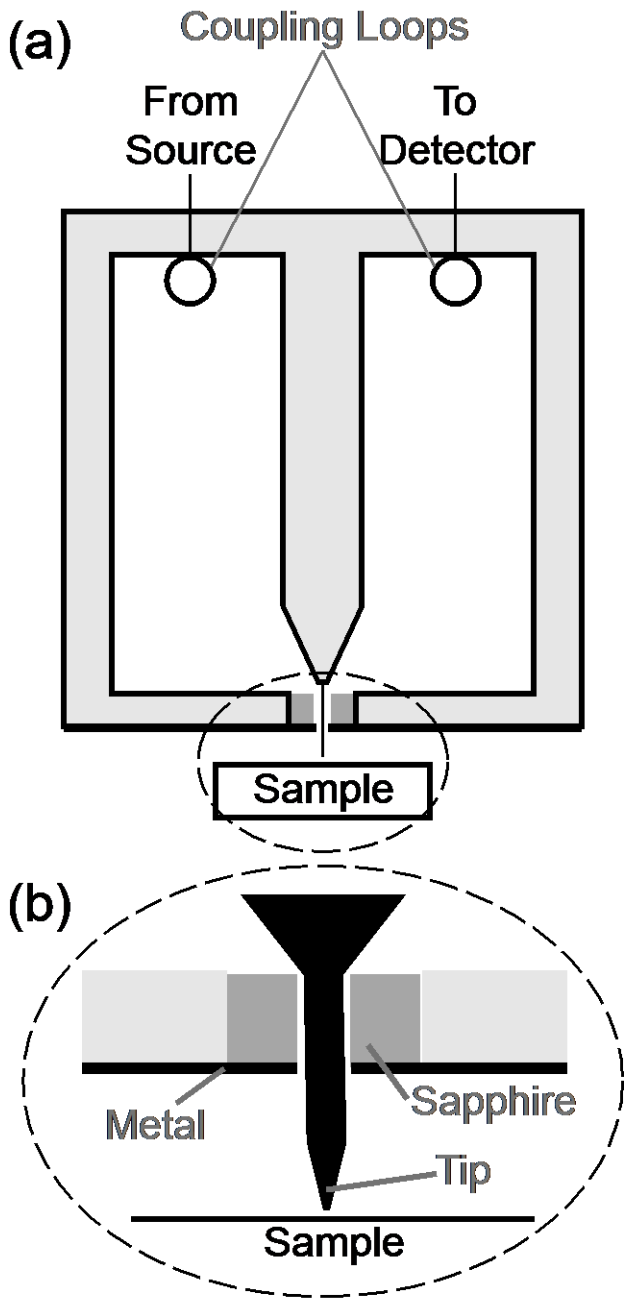
(a)
Coupling Loops
From Source
To Detector
Sample
(b)
Metal
Sapphire
Tip
Sample

Figure 7.6

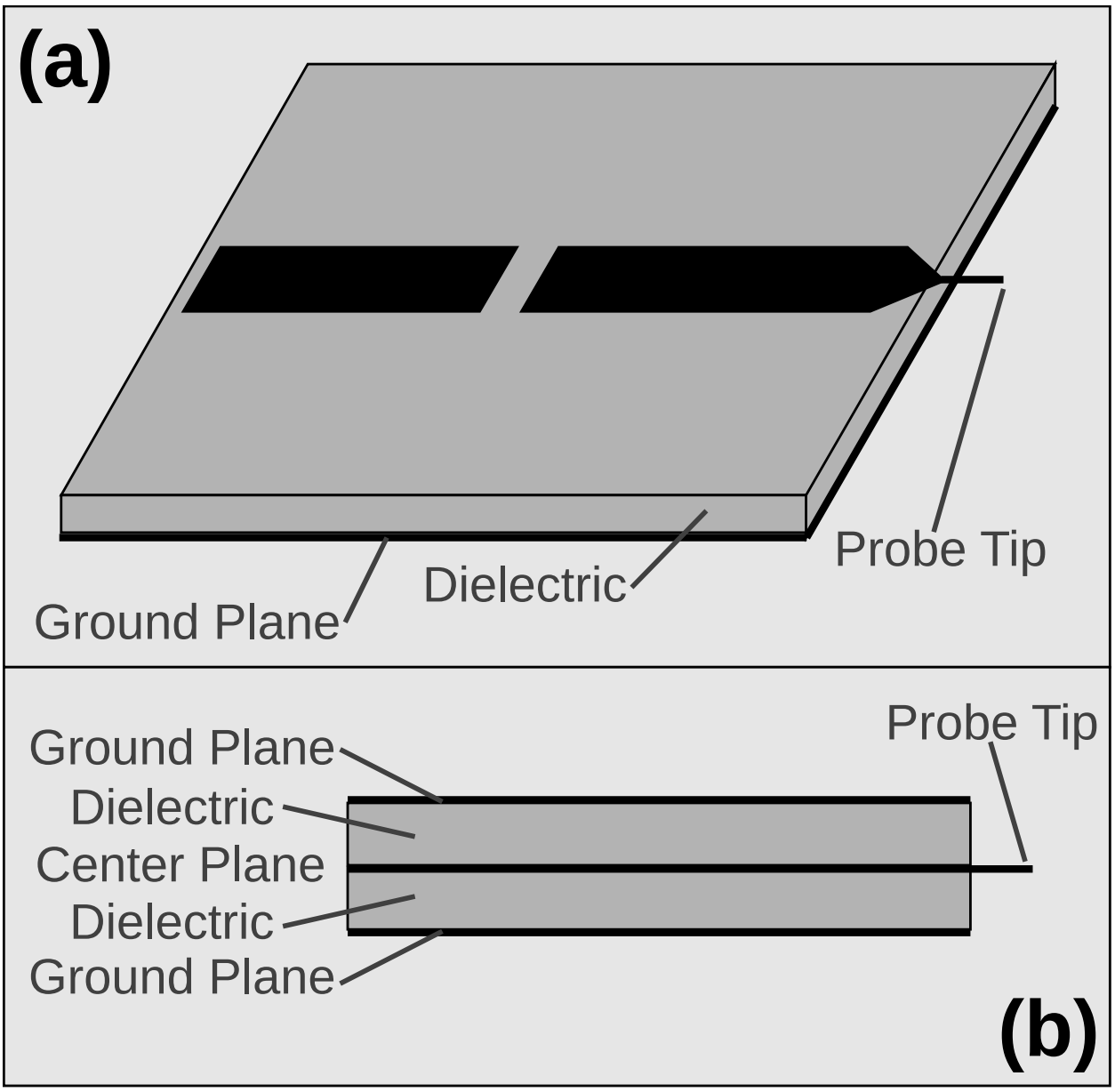
(a)
Probe Tip
Dielectric
Ground Plane
Probe Tip
Ground Plane
Dielectric
Center Plane
Dielectric
Ground Plane
(b)

Figure 7.7

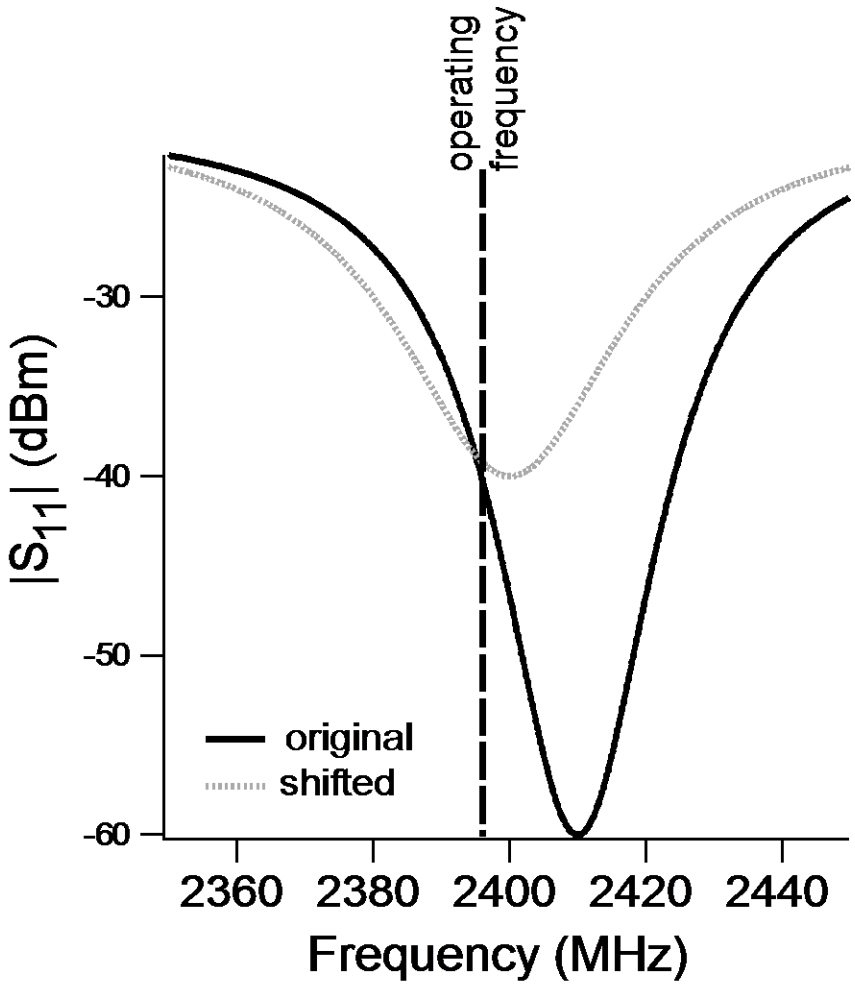
operating
frequency
-30
-40
-50
-60
|S11| (dBm)
original
shifted
2360
2380
2400
2420
2440
Frequency (MHz)

Figure 7.8